ADVANCED MATERIALS
www.advmat.de

Near-Infrared Excitation/Emission and Multiphoton-Induced Fluorescence of Carbon Dots

Di Li, Pengtao Jing, Lihuan Sun, Yang An, Xinyan Shan, Xinghua Lu, Ding Zhou, Dong Han, Dezhen Shen, Yuechen Zhai, Songnan Qu, Radek Zbořil, and Andrey L. Rogach**

Carbon dots (CDs) have significant potential for use in various fields including biomedicine, bioimaging, and optoelectronics. However, inefficient excitation and emission of CDs in both near-infrared (NIR-I and NIR-II) windows remains an issue. Solving this problem would yield significant improvement in the tissue-penetration depth for in vivo bioimaging with CDs. Here, an NIR absorption band and enhanced NIR fluorescence are both realized through the surface engineering of CDs, exploiting electron-acceptor groups, namely molecules or polymers rich in sulfoxide/carbonyl groups. These groups, which are bound to the outer layers and the edges of the CDs, influence the optical bandgap and promote electron transitions under NIR excitation. NIR-imaging information encryption and in vivo NIR fluorescence imaging of the stomach of a living mouse using CDs modified with poly(vinylpyrrolidone) in aqueous solution are demonstrated. In addition, excitation by a 1400 nm femtosecond laser yields simultaneous two-photon-induced NIR emission and three-photon-induced red emission of CDs in dimethyl sulfoxide. This study represents the realization of both NIR-I excitation and emission as well as two-photon- and three-photon-induced fluorescence of CDs excited in an NIR-II window, and provides a rational design approach for construction and clinical applications of CD-based NIR imaging agents.

Owing to their attractive optical properties, small size, low cost, and biocompatibility, carbon dots (CDs) including graphene quantum dots (GQDs) have emerged as promising materials for various applications, such as bioimaging, biomedicine, and optoelectronics.[1] To date, strong photoluminescence (PL) of CDs has mostly been demonstrated in the blue and green spectral regions where a maximum PL quantum yield (QY) of 94% has been obtained.[2] The realization of strong emission of CDs at longer wavelengths than those associated with these regions has been extensively investigated, but remains difficult.[3] This emission is essential for near-infrared (NIR) imaging probes used in in vivo imaging, where low levels of photon scattering, light absorption, and autofluorescence of biological tissues (and, hence, large tissue-penetration depths) are required.[4] For effective imaging, NIR agents should be efficiently excited and capable of emitting light in both NIR windows, namely NIR-I (700–900 nm) or NIR-II (1000–1700 nm).[4a,5] Attempts at reaching the NIR-I window of CDs have, to date, only been described in few publications. Lau and co-workers obtained nitrogen-doped GQDs with a broadband emission of 300–1000 nm, but the corresponding very weak absorption in the NIR region resulted in very weak NIR emission.[6] In another study, CDs with a maximum emission peak at 683 nm and a PL QY of 14% under 420 nm excitation were synthesized via microwave-mediated heating of glutathione in formamide.[7] Similarly, solvothermal treatment of spinach produced CDs with emission at 680 nm and a PL QY of 15% under excitation at 440 nm.[8] Yang and co-workers reported on CDs with emission peaks at 665 and 710 nm and a PL QY of 26% under 540 nm excitation.[9] Zhang and co-workers synthesized S and Se co-doped CDs exhibiting absorption maximum at 526 nm and two emission peaks at 731 and 820 nm with a PL QY of 0.2%.[10] However, those CDs all suffered from the drawback of weak absorption in the NIR region, which renders the realization of strong and efficient NIR

Dr. D. Li, Dr. P. Jing, Dr. D. Zhou, Dr. D. Han, Prof. D. Shen, Y. Zhai, Prof. S. Qu
State Key Laboratory of Luminescence and Applications
Changchun Institute of Optics Fine Mechanics and Physics Chinese Academy of Sciences
3888 Eastern South Lake Road, Changchun 130033, P. R. China
E-mail: qusn@ciomp.ac.cn
L. Sun, Y. An, Prof. X. Shan, Prof. X. Lu
Institute of Physics
Chinese Academy of Sciences
Beijing 100190, P. R. China
The ORCID identification number(s) for the author(s) of this article can be found under https://doi.org/10.1002/adma.201705913.

DOI: 10.1002/adma.201705913

L. Sun, Y. An, Y. Zhai
School of Physical Sciences
University of Chinese Academy of Sciences
Beijing 100190, P. R. China
Prof. R. Zbořil, Prof. A. L. Rogach
Department of Physical Chemistry
Regional Centre of Advanced Technologies and Materials
Palacky University Olomouc
Šlechtitelů 27, Olomouc 783 71, Czech Republic
Prof. A. L. Rogach
Department of Materials Science and Engineering
Centre for Functional Photonics (CFP)
City University of Hong Kong
Kowloon, Hong Kong SAR
E-mail: andrey.rogach@cityu.edu.hk

emission under NIR excitation difficult. Developing a strategy for realizing strong and efficient NIR emission of CDs under excitation in the NIR window is therefore a key challenge for CDs' use in bioimaging applications.

In our previous work,[11] we demonstrated orange emissive CDs from citric acid and urea in dimethylformamide. These CDs exhibited a high PL QY of 46% with a PL peak at 580 nm, owing to the large conjugated sp^2-domains and functionalization of the surface with metal cations. We also demonstrated particle-size modulation of the optical bandgaps of these CDs. The particle sizes were reflected in the dimensions of conjugated sp^2-domains, and the modulation was achieved by controlling the dehydration and carbonization processes occurring between the citric acid and the urea.[12] Herein, we show that an NIR absorption band and enhanced NIR fluorescence can both be realized through surface engineering where these CDs are modified with molecules or polymers rich in sulfoxide/carbonyl groups. CDs dispersed in dimethyl sulfoxide (DMSO) develop an absorption band in the NIR-I region at 715 nm, which yields efficient NIR emission at 760 nm (PL QY reaching 10%), under NIR excitation. The NIR excitation and emission are both important for CDs to realize the in vivo fluorescence imaging. Moreover, two-photon- and three-photon-induced fluorescence are simultaneously realized for CDs in DMSO under excitation of a femtosecond pulse laser in an NIR-II window (1000–1700 nm). Exploiting these superior optical characteristics, in vivo NIR fluorescence imaging using CDs modified with a poly(vinylpyrrolidone) (PVP) aqueous solution is achieved in the stomach of a living mouse. This work demonstrates a first approach for realizing CDs with an NIR absorption band and achieving efficiently NIR emissive CDs with either one-photon excitation in an NIR-I or multiphoton excitation in an NIR-II window for applications in NIR fluorescence imaging and encryption.

The CDs were synthesized as reported in ref. [11], and details are presented in the Supporting Information. The transmission electron microscopy (TEM) image (**Figure 1**a) reveals diameters of 4–11 nm (average size ≈ 6 nm) for the CDs, and well-resolved crystalline lattice fringes characteristic of single particles (see high-resolution TEM (HRTEM) image in the inset of Figure 1a). The interlayer spacing (0.21 nm) corresponds to the *d*-spacing of the graphene $\{1\bar{1}00\}$ planes.[13] Furthermore, atomic force microscopy (AFM) reveals CD particle heights of 1–5 nm (Figure 1b), corresponding to the disk-like morphology of the CDs. AFM-based confocal Raman spectroscopy and imaging of the individual CDs (Figure 1c,d) yield similar Raman signals. These signals are characterized by a disordered (D) band at 1365 cm^{-1} and a sharp band at 1649 cm^{-1} under 532 nm excitation. Under 488 nm excitation, the D band blueshifts to 1371 cm^{-1}, while the other band remains at 1649 cm^{-1} (Figure S1, Supporting Information). Therefore, the excitation-independent band at 1649 cm^{-1} is attributed to the crystalline (G) band, which exhibits E_{2g} symmetry and resists dispersion under different excitation wavelengths. Compared with the typical in-plane vibration (G band) of C atoms at 1580 cm^{-1}, the observed blueshifted G band at 1649 cm^{-1} may have resulted from the presence of highly doped N and O elements (elemental analysis: C, 46.33%; N, 15%; H, 3.25%; and O cal: 35.42%).[14] A typical X-ray powder diffraction (XRD) profile of the CDs (Figure 4a) consists of a relatively sharp peak at ≈27.5°, corresponding to a layer spacing of 3.2 Å in the graphite-like multilayer structure. The broad and weak component at ≈26.8° may be associated with the slightly disordered layers of the CDs.

Optical studies are performed on CDs dispersed in H_2O and in aprotic polar solvents, such as DMSO, *N*,*N*-dimethylformamide (DMF), and *N*-methyl-2-pyrrolidone (NMP). The major absorption band of the CDs in H_2O occurs at a wavelength of 540 nm with a long tail extending into the NIR region (Figure 1e). CD emission occurs in the red region (λ_{max} = 624 nm) under excitation at 561 nm with PL QY of 6% (Figure 1f). In contrast, CDs in DMSO exhibit a redshifted main absorption band at 619 nm, an additional NIR absorption peak at 715 nm, and an enhanced red fluorescence (Figure 1e,f) with a PL QY of 26% (λ_{ex} = 561 nm, λ_{em} = 640 nm). Owing to the NIR absorption band, these CDs also exhibit efficient NIR emission at 760 nm under 732 nm excitation with a PL QY of 10%. Their water counterparts, in contrast, exhibit very weak NIR emission at ≈760 nm under the same excitation conditions (Figure 1g). Enhanced red and NIR emissions of CDs have also been observed in other aprotic polar solutions, namely DMF and NMP (Figure S2, Supporting Information). These solvents have similar electron-acceptor groups (S=O/C=O), which are capable of modifying the surface of the CDs, thereby influencing the optical bandgap and promoting electron transitions under NIR excitation. This is verified by recording the absorption spectra of CDs dispersed in mixed solutions of DMSO and H_2O (Figure S3, Supporting Information). The absorption band occurring at 540 nm for pure H_2O decreases gradually with increasing volume ratio of DMSO to H_2O. However, for pure DMSO, the intensity of the absorption peak at 619 nm increases with the enhanced NIR absorption peak at 715 nm.

The excited state dynamics of CDs in DMSO is investigated via femtosecond transient absorption (TA) spectroscopy. As shown in Figure 1h,i and Figure S4 in the Supporting Information, femtosecond pulse excitation at 580 nm yields two ground-state bleaching (GSB) bands that occur at ≈600–660 nm (GSB1) and 700–800 nm (GSB2) in the TA spectra. The maximum of the GSB1 peak at 625 nm is reached 0.5 ps after excitation and decreases rapidly with increasing delay time of 0.5–12 ps. In contrast, the GSB2 peak at 720 nm increases during the same time period, indicating that charge transfer, from the higher excited state of GSB1 to the lower GSB2 state, can occur. Figure 1i shows the bleach signal kinetics of GSB1 and GSB2. The decay curve at 625 nm is fitted by cubic exponential functions with time constants of 0.94 (29%), 35.38 (24%), and 2402.88 (47%). The TA kinetic trace at 720 nm is fitted by a cubic exponential rise (time constants: 0.15 (66%), 1.23 (5%), and 26.52 (19%) ps) and an exponential decay function (time constant: 851.48 ps (10%)). Consistent with the occurrence of charge transfer between these two excited states, the rapid-decay time constants (0.94 and 35.38 ps) of the GSB1 peak are close to the buildup time constants (1.23 and 26.52 ps) of the GSB2 peak. The rapid-rise component (lifetime: 0.15 ps at 720 nm) is attributed to direct excitation by the pump beam. Similarly, the slow decay processes in GSB1 and GSB2 (lifetimes: 2402.88 and 851.48 ps, respectively) correspond to the radiative transitions. In contrast, the TA spectra of CDs in H_2O (Figure S6, Supporting Information) show that the GSB band at 416–670 nm

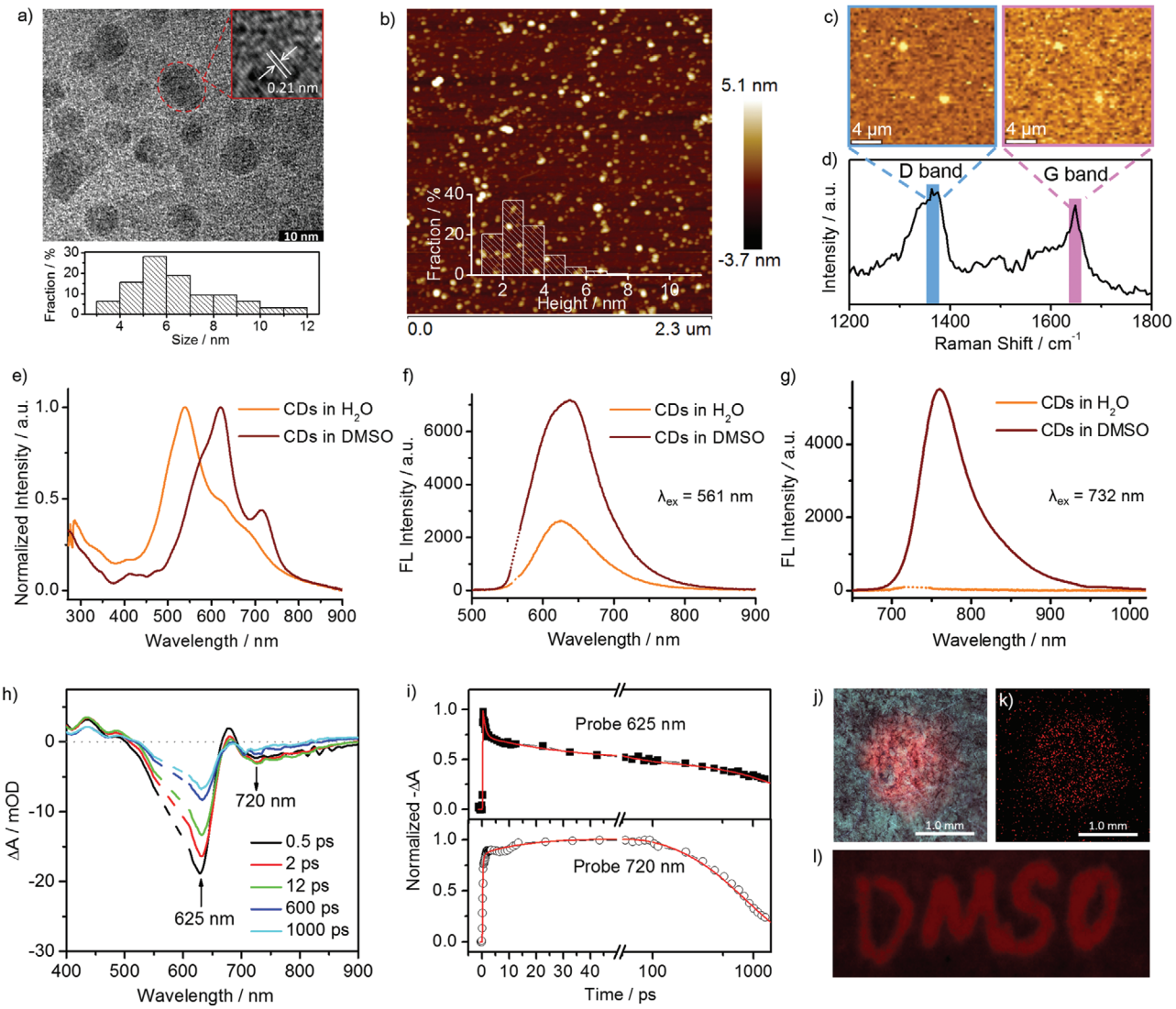

Figure 1. a) TEM image of CDs; inset: HRTEM image of a representative single particle; bottom: size distribution of CDs. b) AFM image of CDs; inset: height distribution of CDs. c) Confocal Raman intensity mapping of D band (left) and G band (right) of two individual CDs, separated by ≈10 µm. d) Typical Raman spectrum of individual CD, with characteristic D and G bands. The mapping intensity in (c) is averaged over 20 cm^{-1}, as indicated by the color bar in (d). e) Absorption spectra of CDs in H_2O and DMSO. f,g) Fluorescence spectra of CDs in H_2O (f) and DMSO (g) under excitation of a 561 and 732 nm laser. The excitation lines at 561 and 732 nm were removed and replaced with dots. h) TA spectra of CDs in DMSO at indicated delay times after excitation at λ_{pump} = 580 nm. i) Bleach signal kinetics of CDs in DMSO for λ_{pump} = 580 nm and probe wavelengths of 625 and 720 nm. j) Fluorescence microscopy photograph and k) EDX mapping of sulfur in lyophilized CD-coated paper within a dripped DMSO droplet. l) Photograph of a CD-coated paper with handwritten characters "DMSO" as viewed under a 732 nm laser with an 800 nm longpass optical filter on the CMOS camera.

is obtained under femtosecond pulse excitation at 580 nm without the appearance of a high-intensity GSB band in the NIR region. The fitted (cubic exponential function) decay time constants at 540 nm are 0.13 (68%), 1.93 (19%), and 962.63 (13%) ps. The large fractions of the rapid decays (lifetimes: 0.13 and 1.93 ps) corresponding to the nonradiative transitions are consistent with the relatively low PL QY (6%) of CDs in H_2O.

The interactions between CDs and DMSO molecules are further considered. During these experiments, the CDs from an aqueous solution are first coated onto paper fibers. The resulting CD-coated paper exhibits only weak fluorescence, as determined under UV illumination. Afterward, a droplet of DMSO is dripped onto the CD-coated paper and then lyophilized, yielding an enhanced red emissive spot that is clearly visible under UV illumination (Figure 1j). Energy dispersive X-ray spectroscopy (EDX) mapping (Figure 1k) reveals sulfur enrichment of the red luminescent region, consistent with the presence of DMSO molecules. This is verified by using a pen dipped in the DMSO solvent to write the characters "DMSO" on the CD-coated paper, which is then lyophilized. These characters are invisible under daylight (Figure S7a, Supporting Information), but are clearly seen under UV excitation (Figure S7b, Supporting Information). Upon excitation with a 732 nm laser, the NIR fluorescent characters "DMSO" are also observed

through a 800 nm longpass optical filter on a complementary metal oxide semiconductor (CMOS) camera (Figure 1l), indicative of the enhanced NIR emission of the DMSO-treated CDs. This DMSO-enhanced red and NIR emission of CDs may constitute a promising means for information encryption.

The aforementioned phenomena have been observed in aprotic polar solutions, such as DMSO, DMF, and NMP, which are molecules rich in electron-acceptor groups. The surface treatment of CDs with such molecules can thus be considered a universal method for developing NIR imaging agents and realizing the CD application in in vivo NIR fluorescence imaging. PVP (Figure S8, Supporting Information) is a highly biocompatible polymer that is widely used in the food industry and in medicine. The structural unit of PVP includes C=O groups (similar to those in NMP), which serve as electron-acceptor bonding sites that can interact with the outer layers and edges of CDs. These interactions yield the desired NIR absorption and emission of CDs: under 732 nm excitation (**Figure 2**a), CDs dispersed in the PVP matrix give rise to an NIR absorption band (maximum intensity at 724 nm) and NIR fluorescence centered at 750 nm. Under this excitation, the characters "CIOMP" handwritten using PVP-treated CDs can be imaged with an 800 nm longpass optical filter (see Figure 2b). Under NIR excitation, CDs in the PVP aqueous solution also exhibit enhanced NIR emission. The intensity of this emission increases with increasing concentration of PVP (Figure S8, Supporting Information) reaching PL QY of 2%, owing to enhanced interactions between CDs and C=O groups in the PVP.

Low cytotoxicity of both bare CDs and PVP-treated CDs are verified via MTT assays. In the presence of CDs (maximum concentration: 400 ppm), the cell viability remains almost the same after 24 h of incubation (Figure S9, Supporting Information). Moreover, the cell viability appears to be higher than 90% after 24 h incubation in the presence of PVP-treated CDs, with PVP concentration ranging from 1 to 100 mg mL^{-1} and 200 ppm CDs (Figure S10, Supporting Information). In order to confirm the feasibility of imaging in physiological environment such as gastric acid environment for PVP-treated CDs, the emission properties of CD/PVP aqueous solution are examined under 671 nm excitation for the neutral and strongly acidic pH; the NIR fluorescence intensity does not decrease when pH changes from 7 to 1 (Figure S11, Supporting Information). Real-time in vivo NIR fluorescence imaging is performed using a CD/PVP aqueous solution and a CMOS camera coupled with a 750 nm longpass optical filter. After a gavage injection of 200 µL CD/PVP aqueous solution (CD 500 µg mL^{-1}, PVP 500 mg mL^{-1}), enhanced NIR fluorescence (Figure 2c,d) occurs in the stomach of the mouse under 671 nm laser excitation (irradiation power density: 4.8 mW cm^{-2}). This power density (much lower than the safe exposure limit of 200 mW cm^{-2} at 671 nm[15]) and bright fluorescence signal in the mouse stomach demonstrate the in vivo NIR imaging ability of CDs in PVP solution. The deep-tissue penetration capability with a potential for NIR bioimaging application is also revealed. Different to the PVP-treated CDs (CD 1 mg mL^{-1}, PVP 500 mg mL^{-1}), CD (1 mg mL^{-1}) aqueous solution and PVP (500 mg mL^{-1}) aqueous solution in the stomach of mice could not be imaged under 671 nm excitation, because of their inefficient NIR excitation and emission (Figure S12, Supporting Information). Under 732 nm laser excitation, bright NIR fluorescence signal from the PVP-treated CDs (CD 1 mg mL^{-1}, PVP 500 mg mL^{-1}) in the stomach of the mouse could easily be distinguished from the background through the 800 nm longpass optical filter, so that the distribution of PVP-treated CDs in the digestive system of the mouse can be real-time tracked (Figure S13, Supporting Information).

Moreover, in vivo NIR fluorescence imaging using PVP-treated CDs can also be realized by another injection routes, such as subcutaneous and tail intravenous injection. Figure S14

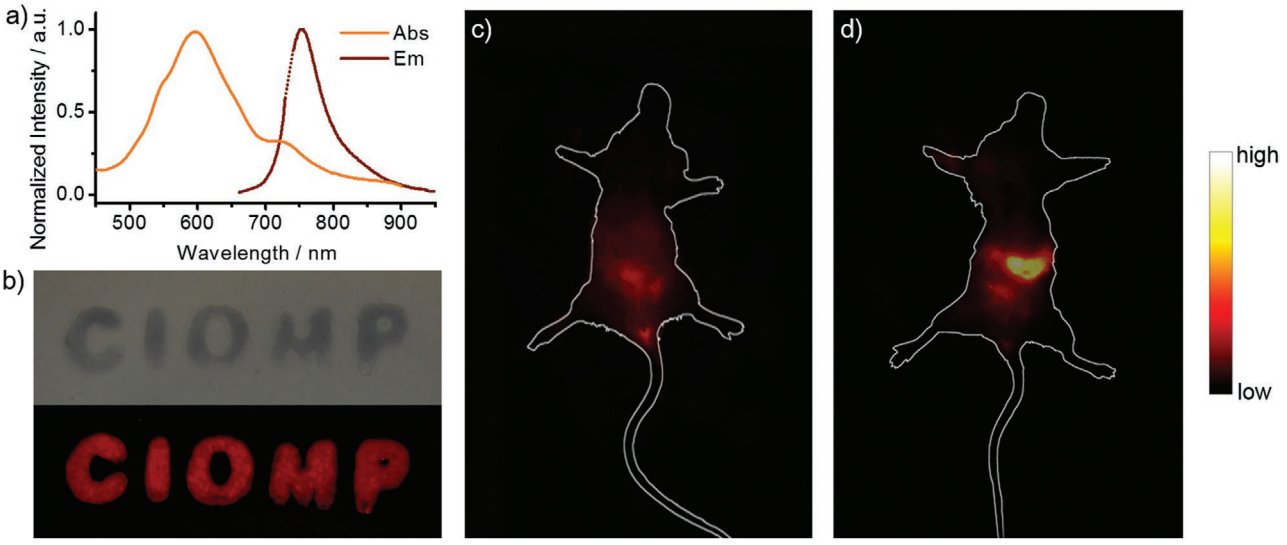

Figure 2. a) Absorption and PL spectra of CD/PVP film (signal of 732 nm laser was removed and replaced with dots). b) Photograph of characters "CIOMP" written by using CD/PVP ink in daylight (upper) and a fluorescence image through an 800 nm longpass optical filter under excitation of a 732 nm laser (lower). c,d) In vivo NIR fluorescence images of a mouse before (c) and after (d) gavage injection of CDs in PVP aqueous solution (Ex: 671 nm, Em: 750 nm longpass optical filter/200 ms).

in the Supporting Information shows NIR fluorescence in the body of a mouse, which is subcutaneously injected with CD/PVP aqueous solution under the irradiation with 671 and 732 nm laser. After tail intravenous injection, enhanced NIR fluorescence occurs around the body under 671 nm excitation and shows the biodistribution of PVP-treated CDs in real time (Figure S15, Supporting Information).

According to previous studies, under 800, 850, or 880 nm femtosecond pulsed laser (fs-laser) excitation, several types of CDs showed two-photon-induced fluorescence in the visible and NIR region.[7,9,10,16] CDs in DMSO exhibit strong absorption in the red and NIR regions. Therefore, in this work, a fs-laser operating in the NIR-II window (wavelength: 1.0–1.7 µm) is used as the excitation source to investigate the multi-photon-induced fluorescence properties of the CDs. Excitation by a 1200 nm fs-laser yields two emission bands (peaked at 654 and 766 nm) for CDs in DMSO (**Figure 3**a). Figure 3b shows the polynomial fitting (plotted on logarithmic scales) of the emission intensity as a function of the input excitation intensity. The slopes of the plots corresponding to emissions at 654 and 766 nm are consistent with the occurrence of a two-photon excitation process. In contrast, CDs in H_2O exhibit relatively weak fluorescence at 650 nm when excited by the 1200 nm fs-laser (Figure S16, Supporting Information). Multiphoton-induced emission spectra for CDs in DMSO are obtained (see Figure 3c) at various excitation intensities of the excitation source at 1400 nm. These spectra consist of two emission peaks (at ≈654 and 768 nm) with intensities that increase nonlinearly with increasing laser power. The intensity at 654 nm increases more rapidly than the emission intensity at 768 nm. Therefore, the primary emission maximum shifts from 768 to 654 nm when the excitation intensity is increased. The emission intensity as a function of the input excitation intensity has a slope of three for emission at 654 nm, indicating a cubic dependence typical of three-photon excitation. A slope of two for emission at 768 nm is consistent with the occurrence of a two-photon excitation process (Figure 3d). To the best of our knowledge, this represents the first-ever simultaneous realization of two-photon- and three-photon-induced fluorescence of CDs excited in an NIR-II window. Lower levels of scattering, absorption, and tissue autofluorescence occur in NIR-II than in the NIR-I window.[17] Similarly, a low amount of crosstalk occurs between the exciting laser (NIR-II) and the detection region (NIR-I). Therefore, surface engineering of CDs with S=O/C=O groups constitutes a promising technique for efficient in vivo multi-photon fluorescence bioimaging.

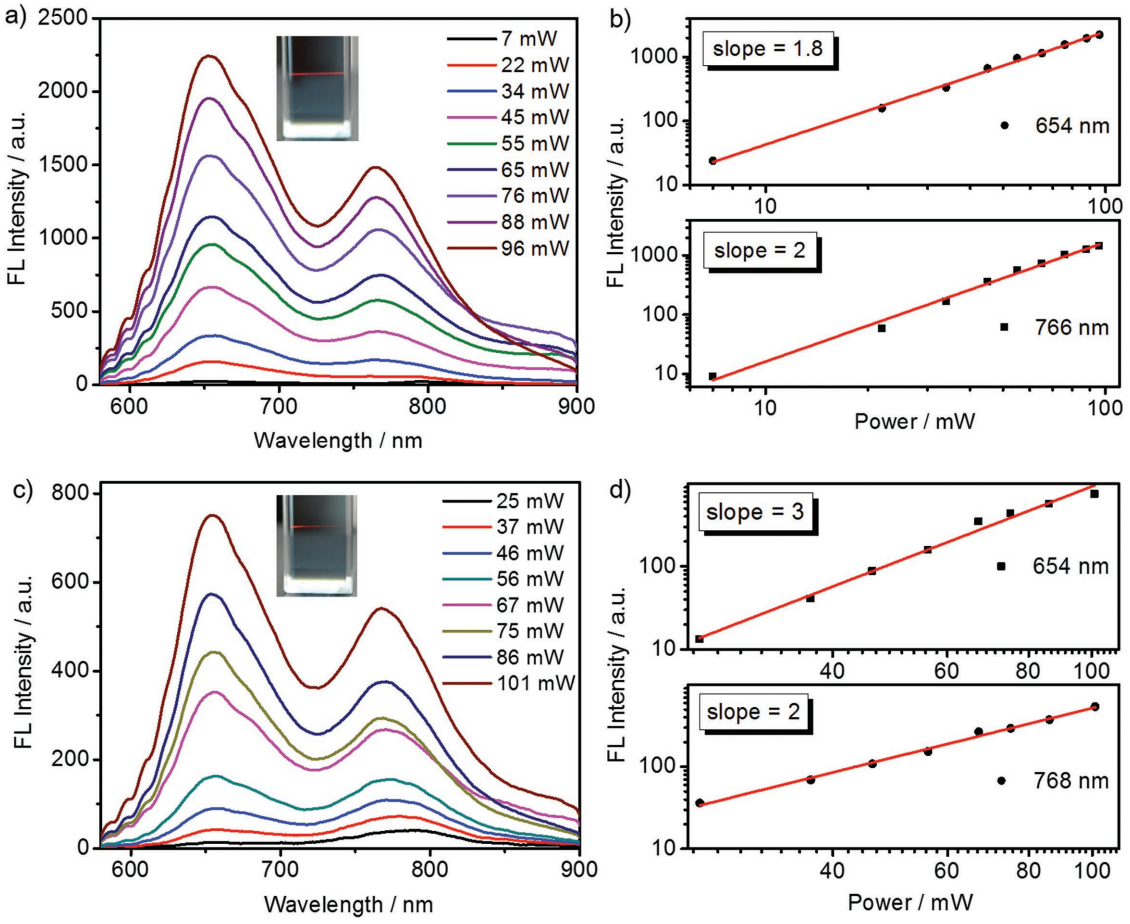

Figure 3. Fluorescence spectra obtained for multiphoton excitation associated with incident intensities at: a) 1200 nm excitation (inset: photograph showing excitation at 1200 nm and 22 mW) and c) 1400 nm excitation (inset: photograph showing excitation at 1400 nm and 46 mW). Power dependence of emission (shown on logarithmic scales) at: b) 1200 nm excitation and d) 1400 nm excitation.

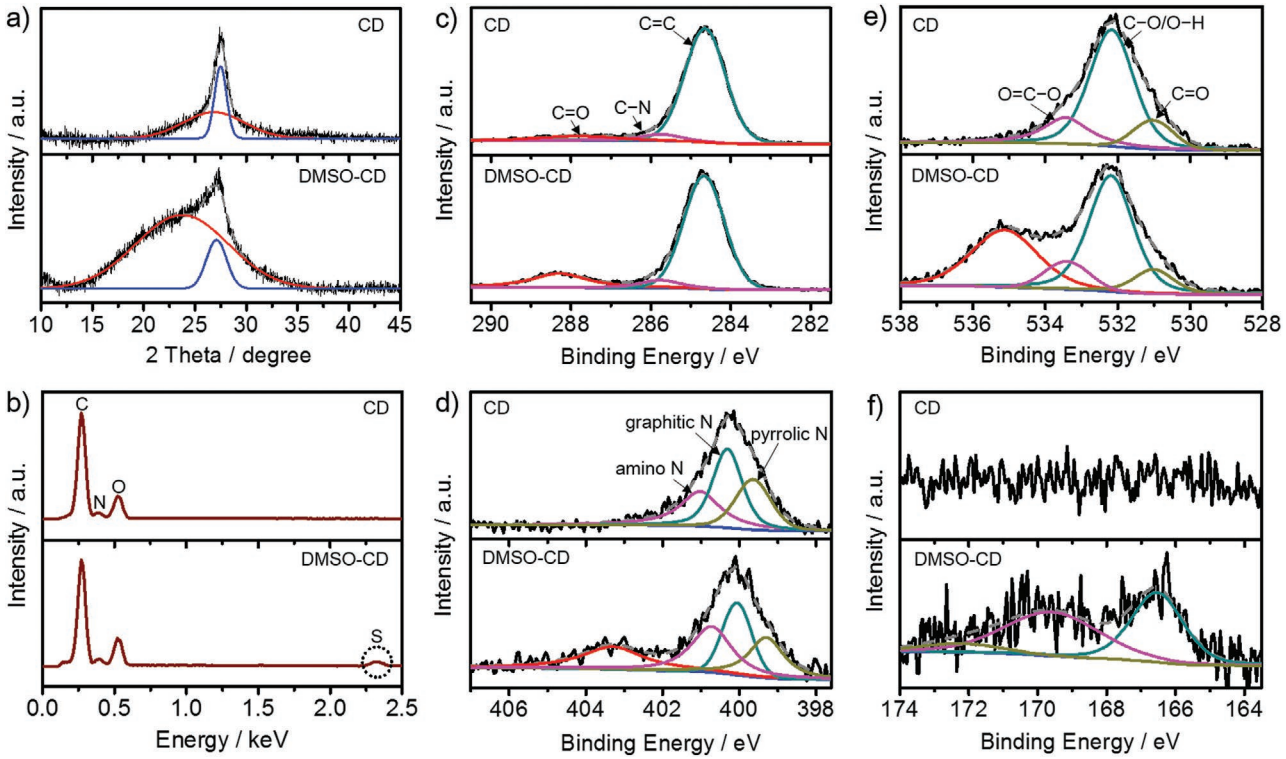

Figure 4. a) XRD profiles and b) EDX spectra of bare CDs and DMSO-treated CDs. c–f) High-resolution C 1s (c), N 1s (d), O 1s (e), S 2p (f) XPS spectra of bare CDs (upper frames) and DMSO-treated CDs (lower frames).

The surface modification of DMSO-treated CDs is investigated via XRD, EDX, X-ray photoelectron spectroscopy (XPS), and Fourier transform infrared (FT-IR) spectroscopy. DMSO-treated CD powders are prepared by dissolving CDs in DMSO (concentration: 2 mg mL^{-1}) and lyophilizing the solution thoroughly to remove the unbonded DMSO. Compared with the XRD pattern of bare CDs, the pattern of the DMSO-treated CDs consists of a (i) broad peak that is dominant, broader, and centered at a smaller diffraction angle of 23.7°, and (ii) sharp peak that is significantly weaker, broader, and centered at a smaller diffraction angle of 27.1° (**Figure 4**a). This suggests that the ordered layer stacking in the basal planes of the CDs is partially destroyed by the DMSO treatment. The EDX spectra of CDs and DMSO-treated CDs are characterized by C, N, and O peaks centered at 0.27, 0.39, and 0.53 eV (see Figure 4b). The S peak at 2.32 eV occurs only for the DMSO-treated CDs and is, therefore, consistent with the presence of DMSO molecules (with a weight ratio of 21%). The high-resolution C 1s, N 1s, and O 1s XPS spectra (Figure 4c–f) confirm the existence of C=C (284.6 eV), C−N (285.8 eV), and C=O (287.8 eV) for C 1s; pyrrolic N (399.6 eV), graphitic N (400.3 eV), and amino N (401 eV) for N 1s; C=O (531 eV), C−O/O−H (532.2 eV), and O=C−O (533.4 eV) for O 1s in CDs.[18] A comparison of high-resolution C 1s, N 1s, O 1s, and S 2p XPS spectra reveals that the DMSO treatment results in changes in the surface-element chemical environment of the CDs. For example, the peak of C=O occurring at 287.8 eV in the bare CDs shifts to a higher binding energy of 288.3 eV in the DMSO-treated CDs (see Figure 4c). Similarly, as Figure 4d–f shows, the oxidic N (403.3 eV) and O (535.1 eV), and S 2p3/2 (172.2, 169.6, and 166.5 eV) peaks occur only for the DMSO-treated CDs. XPS results show that DMSO molecules are anchored on the surface of the CDs, leading to increased oxidation of C and N. Absorption bands at 3330–3650 cm^{-1} and 1550–1750 cm^{-1} in the FT-IR spectra of both the bare- and DMSO-treated CDs correspond to υ(O−H)/υ(N−H) and υ(C=O)/ν(C=N)/δ(N−H), respectively, which are associated with carboxyl, amino, and aromatic CN heterocycles.[19] The characteristic absorption peak of δ(N−H) occurs at 1587 cm^{-1} for the bare CDs and at a smaller wavenumber of 1548 cm^{-1} for their DMSO-treated counterparts. In addition, the DMSO-treated CDs give rise to an absorption band, υ(S=O), with maximum intensity occurring at 1025 cm^{-1} (Figure S17, Supporting Information).[20] The FT-IR results indicate that hydrogen bonds are formed between S=O in the DMSO molecules and N−H groups on the edges of the CDs.[21] The combined XRD, EDX, XPS, and FT-IR data suggest that electron-acceptor groups, such as S=O in DMSO or C=O in DMF and NMP, can interact with both the N-, O-doped carbon-based layers and N−H groups on the surface of the CDs. These interactions may occur via partial oxidation bonding and hydrogen bonding, yielding modulated optical properties of the CDs and, in turn, an emerging NIR absorption band and enhanced NIR emission.

Based on the results above, a possible mechanism for surface engineering aimed at generating the NIR absorption band and enhanced NIR emissions from CDs is illustrated in **Figure 5**. S=O/C=O groups, present in DMSO/DMF/NMP, interact with the surface of CDs. These CDs have a layered structure and the constituent outer layers and edges

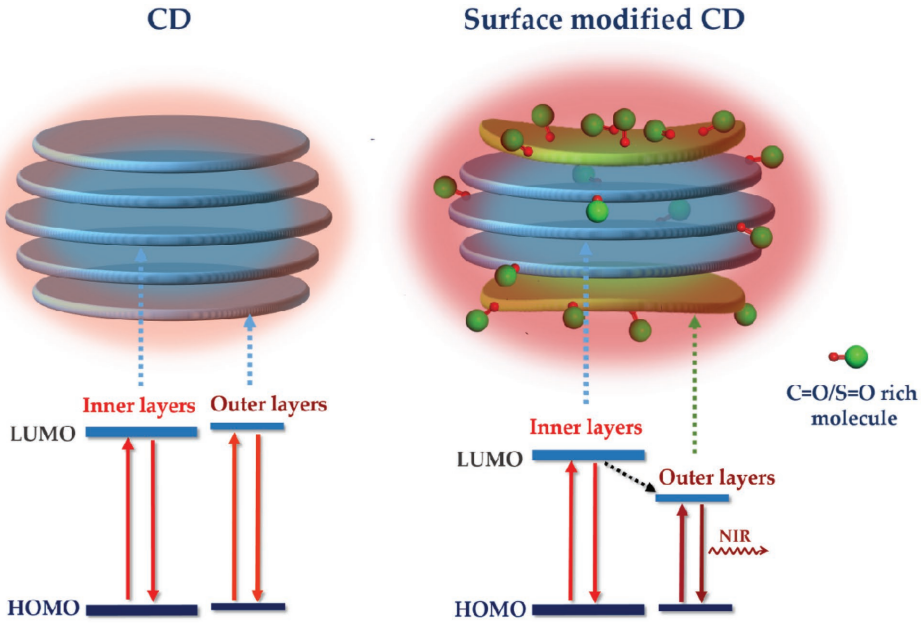

Figure 5. Schematic of structure and energy level alignments of nontreated CDs (left column) and CDs modified with S=O/C=O-rich molecules (right column). The red (oxygen atom) and green double-bonded balls represent the C=O/S=O-rich molecule.

may consist of bonding sites. The aforementioned interactions result in increased surface oxidation (particularly for the outer layers), which leads to a reduction in the lowest unoccupied molecular orbital (LUMO) level and yields the red-shifted absorption band.[3c,22] This suggests that bonding with molecules rich in S=O/C=O groups on the basal planes of the outer layers results in a decrease in the co-planarity and the interlayer interactions of the outer layers. The ordered layered structure of the CDs is thereby disrupted, as indicated by the corresponding XRD patterns. The consequent nonconjugation of the outer layers and inner layers is reflected in the occurrence of additional discrete energy levels in the CDs modified with S=O/C=O-rich molecules. Owing to the increased surface oxidation, the LUMO levels of the outer layers are lower than those of the inner layers, thereby resulting in the NIR absorption band and NIR emission of the CDs. Considering the small separation, charge transfers from the inner layers to the outer layers are possible and may contribute to the NIR emission, as observed via TA spectroscopy.

To conclude, efficient NIR emission for CDs excited in an NIR-I window ($\lambda_{abs} \approx 715$–$724$ nm, $\lambda_{em} \approx 750$–760 nm, QY = 10%) has been realized through surface engineering of molecules or polymers rich in sulfoxide/carbonyl groups. These groups are attached to the outer layers and the edges of the CDs, thereby resulting in increased surface oxidation and the occurrence of discrete energy levels. This contributes to the NIR absorption band and enhanced NIR fluorescence. The surface-modified CDs are successfully applied for in vivo NIR fluorescence imaging and NIR-imaging information encryption. Two-photon-induced NIR emission and three-photon-induced red emission are first-ever simultaneously observed for CDs in DMSO under excitation of an NIR-II (1400 nm) fs-laser. This work demonstrates the attractive optical features and promising applications of CDs in the NIR region, and provides a rational design approach for developing CD-based NIR imaging agents.

Experimental Section

Detailed experimental materials and methods can be found in the Supporting Information.

Supporting Information

Supporting Information is available from the Wiley Online Library or from the author.

Acknowledgements

The authors gratefully acknowledge the support by the National Natural Science Foundation of China (No. 51602304), the Jilin Province Science and Technology Research projects (Nos. 20170101191JC, 20170101042JC, 20160520008JH, and 20150519003JH), the Youth Innovation Promotion Association of Chinese Academy of Sciences, the Open Project Program of the State Key Laboratory of Supramolecular Structure and Materials in Jilin University (No. sklssm201712), the Ministry of Science and Technology of China (No. 2012CB933002), the Open Project Program of State Key Laboratory of Polymer Physics and Chemistry, Changchun Institute of Applied Chemistry, Chinese Academy of Sciences, the Strategic Priority Research Program (B) of the Chinese Academy of Sciences (No. XDB07030100), the Nanomaterials and Nanotechnologies for Environment Protection and Sustainable Future (NanoEnviCz, LM2015073), and the project LO1305 of the Ministry of Education, Youth and Sports of the Czech Republic. The authors thank CNI Laser for providing the 561 and 671 nm diode laser.

Conflict of Interest

The authors declare no conflict of interest.

Keywords

carbon dots, multiphoton-induced fluorescence, near-infrared absorption, near-infrared fluorescence, surface engineering

Received: October 10, 2017
Revised: December 12, 2017
Published online: February 7, 2018

[1] a) V. Georgakilas, J. A. Perman, J. Tucek, R. Zboril, *Chem. Rev.* **2015**, *115*, 4744; b) G. E. LeCroy, S.-T. Yang, F. Yang, Y. Liu, K. A. S. Fernando, C. E. Bunker, Y. Hu, P. G. Luo, Y.-P. Sun, *Coord. Chem. Rev.* **2016**, *320*, 66; c) K. Hola, Y. Zhang, Y. Wang, E. P. Giannelis, R. Zboril, A. L. Rogach, *Nano Today* **2014**, *9*, 590; d) S. N. Baker, G. A. Baker, *Angew. Chem., Int. Ed.* **2010**, *49*, 6726; e) C. Ding, A. Zhu, Y. Tian, *Acc. Chem. Res.* **2014**, *47*, 20; f) S. Y. Lim, W. Shen, Z. Gao, *Chem. Soc. Rev.* **2015**, *44*, 362; g) X. T. Zheng, A. Ananthanarayanan, K. Q. Luo, P. Chen, *Small* **2015**, *11*, 1620; h) X. Li, M. Rui, J. Song, Z. Shen, H. Zeng, *Adv. Funct. Mater.* **2015**, *25*, 4929.

[2] a) R. Ye, C. Xiang, J. Lin, Z. Peng, K. Huang, Z. Yan, N. P. Cook, E. L. G. Samuel, C.-C. Hwang, G. Ruan, G. Ceriotti, A.-R. O. Raji, A. A. Martí, J. M. Tour, *Nat. Commun.* **2013**, *4*, 2943; b) L. Wang, Y. Wang, T. Xu, H. Liao, C. Yao, Y. Liu, Z. Li, Z. Chen, D. Pan, L. Sun, M. Wu, *Nat. Commun.* **2014**, *5*, 5357; c) X. Wang, L. Cao, S.-T. Yang, F. Lu, M. J. Meziani, L. Tian, K. W. Sun, M. A. Bloodgood, Y.-P. Sun, *Angew. Chem., Int. Ed.* **2010**, *49*, 5310; d) Z. Xie, F. Wang, C.-Y. Liu, *Adv. Mater.* **2012**, *24*, 1716; e) D. Qu, M. Zheng, L. Zhang, H. Zhao, Z. Xie, X. Jing, R. E. Haddad, H. Fan, Z. Sun, *Sci. Rep.* **2014**, *4*, 5294.

[3] a) J. Ge, M. Lan, B. Zhou, W. Liu, L. Guo, H. Wang, Q. Jia, G. Niu, X. Huang, H. Zhou, X. Meng, P. Wang, C.-S. Lee, W. Zhang, X. Han, *Nat. Commun.* **2014**, *5*, 4596; b) J. Ge, Q. Jia, W. Liu, L. Guo, Q. Liu, M. Lan, H. Zhang, X. Meng, P. Wang, *Adv. Mater.* **2015**, *27*, 4169; c) H. Ding, S.-B. Yu, J.-S. Wei, H.-M. Xiong, *ACS Nano* **2016**, *10*, 484; d) K. Jiang, S. Sun, L. Zhang, Y. Lu, A. Wu, C. Cai, H. Lin, *Angew. Chem., Int. Ed.* **2015**, *54*, 5360; e) L. Pan, S. Sun, A. Zhang, K. Jiang, L. Zhang, C. Dong, Q. Huang, A. Wu, H. Lin, *Adv. Mater.* **2015**, *27*, 7782; f) S. Sun, L. Zhang, K. Jiang, A. Wu, H. Lin, *Chem. Mater.* **2016**, *28*, 8659; g) F. Yuan, Z. Wang, X. Li, Y. Li, Z. a. Tan, L. Fan, S. Yang, *Adv. Mater.* **2017**, *29*, 1604436; h) Z. Wang, F. Yuan, X. Li, Y. Li, H. Zhong, L. Fan, S. Yang, *Adv. Mater.* **2017**, *29*, 1702910.

[4] a) G. Hong, A. L. Antaris, H. Dai, *Nat. Biomed. Eng.* **2017**, *1*, 0010; b) R. Weissleder, *Nat. Biotechnol.* **2001**, *19*, 316.

[5] V. J. Pansare, S. Hejazi, W. J. Faenza, R. K. Prud'homme, *Chem. Mater.* **2012**, *24*, 812.

[6] L. Tang, R. Ji, X. Li, G. Bai, C. P. Liu, J. Hao, J. Lin, H. Jiang, K. S. Teng, Z. Yang, S. P. Lau, *ACS Nano* **2014**, *8*, 6312.

[7] L. Pan, S. Sun, L. Zhang, K. Jiang, H. Lin, *Nanoscale* **2016**, *8*, 17350.

[8] L. Li, R. Zhang, C. Lu, J. Sun, L. Wang, B. Qu, T. Li, Y. Liu, S. Li, *J. Mater. Chem. B* **2017**, *5*, 7328.

[9] S. Lu, L. Sui, J. Liu, S. Zhu, A. Chen, M. Jin, B. Yang, *Adv. Mater.* **2017**, *29*, 1603443.

[10] M. Lan, S. Zhao, Z. Zhang, L. Yan, L. Guo, G. Niu, J. Zhang, J. Zhao, H. Zhang, P. Wang, G. Zhu, C.-S. Lee, W. Zhang, *Nano Res.* **2017**, *10*, 3113.

[11] S. Qu, D. Zhou, D. Li, W. Ji, P. Jing, D. Han, L. Liu, H. Zeng, D. Shen, *Adv. Mater.* **2016**, *28*, 3516.

[12] Z. Tian, X. Zhang, D. Li, D. Zhou, P. Jing, D. Shen, S. Qu, R. Zboril, A. L. Rogach, *Adv. Opt. Mater.* **2017**, *5*, 1700416.

[13] T.-F. Yeh, C.-Y. Teng, S.-J. Chen, H. Teng, *Adv. Mater.* **2014**, *26*, 3297.

[14] a) W. Yuan, L. Fang, Z. Feng, Z. Chen, J. Wen, Y. Xiong, B. Wang, *J. Mater. Chem. C* **2016**, *4*, 4778; b) F. Liu, M.-H. Jang, H. D. Ha, J.-H. Kim, Y.-H. Cho, T. S. Seo, *Adv. Mater.* **2013**, *25*, 3657.

[15] R. Matthes, C. P. Cain, D. Courant, D. A. Freund, B. A. Grossman, P. A. Kennedy, D. J. Lund, M. A. Mainster, A. A. Manenkov, W. J. Marshall, R. McCally, B. A. Rockwell, D. H. Sliney, P. A. Smith, B. E. Stuck, S. A. Tell, M. L. Wolbarsht, G. I. Zheltov, F. Cheney, L. McLin, J. Ness, K. Schulmeister, R. M. Steinman, E. Sutter, H. Zwick, I. C. N.-I. R. Protect, *Health Phys.* **2000**, *79*, 431.

[16] a) Q. Liu, B. Guo, Z. Rao, B. Zhang, J. R. Gong, *Nano Lett.* **2013**, *13*, 2436; b) L. Cao, X. Wang, M. J. Meziani, F. Lu, H. Wang, P. G. Luo, Y. Lin, B. A. Harruff, L. M. Veca, D. Murray, S.-Y. Xie, Y.-P. Sun, *J. Am. Chem. Soc.* **2007**, *129*, 11318; c) S. Lu, G. Xiao, L. Sui, T. Feng, X. Yong, S. Zhu, B. Li, Z. Liu, B. Zou, M. Jin, J. S. Tse, H. Yan, B. Yang, *Angew. Chem., Int. Ed.* **2017**, *56*, 6187.

[17] A. M. Smith, M. C. Mancini, S. Nie, *Nat. Nanotechnol.* **2009**, *4*, 710.

[18] S. Liu, J. Tian, L. Wang, Y. Zhang, X. Qin, Y. Luo, A. M. Asiri, A. O. Al-Youbi, X. Sun, *Adv. Mater.* **2012**, *24*, 2037.

[19] a) D. Li, D. Han, S.-N. Qu, L. Liu, P.-T. Jing, D. Zhou, W.-Y. Ji, X.-Y. Wang, T.-F. Zhang, D.-Z. Shen, *Light: Sci. Appl.* **2016**, *5*, e16120; b) S. Zhu, Q. Meng, L. Wang, J. Zhang, Y. Song, H. Jin, K. Zhang, H. Sun, H. Wang, B. Yang, *Angew. Chem., Int. Ed.* **2013**, *52*, 3953; c) S. Qu, X. Wang, Q. Lu, X. Liu, L. Wang, *Angew. Chem., Int. Ed.* **2012**, *51*, 12215.

[20] M. Meade, K. Hickey, Y. McCarthy, W. Earle Waghorne, M. R. Symons, P. P. Rastogi, *J. Chem. Soc., Faraday Trans.* **1997**, *93*, 563.

[21] J. Joseph, E. D. Jemmis, *J. Am. Chem. Soc.* **2007**, *129*, 4620.

[22] L. Bao, C. Liu, Z.-L. Zhang, D.-W. Pang, *Adv. Mater.* **2015**, *27*, 1663.